IEEE Access
Multidisciplinary | Rapid Review | Open Access Journal

Received September 26, 2019, accepted October 15, 2019, date of publication October 25, 2019, date of current version January 10, 2020.

Digital Object Identifier 10.1109/ACCESS.2019.2949657

A High-Resolution Imaging Method for Strip-Map SAR With Missing Data

HUAJUN DUAN, DAIYIN ZHU, AND TIANSHUN XIANG

College of Electronic and Information Engineering, Nanjing University of Aeronautics and Astronautics, Nanjing 210016, China

Corresponding author: Huajun Duan (dhj5816@sina.com)

This work was supported in part by the National Key Research and Development Program of China under Grant 2017YFB0502700, in part by the Fundamental Research Funds for the Central Universities under Grant NZ2016105, in part by the National Natural Science Foundation of China under Grant 61671240, in part by the Aeronautical Science Foundation of China under Grant 20162052019, and in part by the Jiangsu Innovation Program for Graduate Education under Grant KYLX16_0372.

ABSTRACT Due to the long aperture, the high-resolution imaging for strip-map SAR with missing data is a challenge, in which the range migration correction and phase error correction are challenging. In this paper, a high-resolution imaging method of this type of data based on compressed sensing (CS) is proposed, which divides the strip-map data into several sub-apertures restored by CS and recombined to the strip-map data. The basis matrix and the measurement matrix for CS are deduced. The sub-aperture data is autofocused by the Projection Approximation Subspace Tracking (PAST) algorithm to meet the sparse requirement for the reconstructed image and the intact phase error data is restored by CS in order to combine the sub-apertures. A high-resolution image of the restored data can be obtained by conventional imaging method which performs range migration and autofocus.

INDEX TERMS Synthetic aperture radar, compressed sensing, PAST algorithm, missing data, high-resolution imaging.

I. INTRODUCTION

Synthetic Aperture Radar (SAR) can obtain high-resolution images in day/night and all-weather, so it has been widely used in both the military and the civil application. In practice, the electromagnetic wave transmitted or received by radar is vulnerable to interference, which often results in damaged or missing echo pulses. If we set the damaged or missing data to zero and image the echo data by conventional imaging method, the image quality will degrade to some extent [1], [2]. Therefore, it is significant to improve the image quality of such data [3], [4], which has much practical value in engineering application, for example, the helicopter SAR echo with pulses interrupted by the rotor.

There are many methods to recover the missing data. The first kind is interpolation [5], which can recover the missing data by interpolating based on the good data in the neighborhood of the missing data. But, when the spectrum of data is aliasing or the number of the continuous missing data is large, the result isn't ideal. The second kind is linear prediction and extrapolation [6]–[8]. However, this algorithm is sensitive to prediction model and signal to clutter ratio (SCR), its recovery ability will exponentially decay when the missing data is large. The third kind is the spectrum estimation (e.g. GAPES [1], [2], [9], [10] and MIAA [11] et al.). It is a nonparametric spectrum estimation method with the advantage of high robustness without affected by model parameter. It has strong restoration ability for 1-D signal or small illuminated scene. Nevertheless, it needs a lot of matrix inversions and multiple iterations which is hard to implement in 2-D SAR data of large size.

Compressed Sensing (CS) [12]–[14] is a novel signal reconstruction algorithm. As long as the signal satisfies the sparse condition at a certain domain, the time domain signal can be sampled at a frequency far below the sampling frequency demanded by the Nyquist Law. The original signal is likely to be restored perfectly using compressed sensing algorithms. When the CS theory is proposed, many scholars study the imaging methods of sparse frequency [15], [16] and azimuth sparse aperture [17]–[20]. In [21], a 2-D sparse sampling method was proposed to reduce the computational burden and the complexity of sparse matrix, which uses sub-block processing in range. After obtaining the sub-block images, the complete image was formed by image

The associate editor coordinating the review of this manuscript and approving it for publication was Qingchun Chen.

mosaicking. All the above mentioned imaging methods are based on spotlight mode data, and the current hardware can meet the computational requirements of reconstruction because of the small data matrix in this mode. Literature [22] studied the CS processing method of sparse aperture SAR for strip-map mode, which was based on the R-D imaging algorithm. This method just corrected the range walk without range curvature correction and phase error compensation, leading to degrade image resolution.

At present, the processing difficulties mainly include four aspects for strip-map SAR with missing data. The first is the large amount of data, which leads to the image reconstruction computational complexity far beyond current hardware computational ability. The second is that the range migration correction must be essentially considered because of the long strip-map aperture, otherwise the image resolution will be degraded. The third is the phase error compensation. The pulse interval is non-uniform for the missing data, so the pulses can't be transformed into frequency domain, and the performance of the conventional autofocusing algorithms is limited to a certain extent. Because the SAR signal is a 2-D frequency modulated signal which can't meet the sparse requirements of CS theory as a result of its wide Fourier spectrum. The fourth problem is that we can't restore the missing data directly in the frequency domain.

To solve the above difficulties, this paper proposes a reconstruction method based on CS for missing data. First, the strip-map data is divided into several sub-apertures, which significantly improves the computational efficiency. The sub-aperture missing data is restored by CS and recombined to the strip-map data. Second, each sub-aperture data is transformed into the image domain by preprocessing and CS is utilized to reconstruct the sub-image. After that, the original data can be restored. Third, each sub-aperture data is autofocused before reconstructing image in order to meet the sparse requirement of CS theory. Fourth, the compensatory phase error signal is restored by CS in order to ensure the sub-aperture recombining without ghost images. Finally, the range migration of the missing data is corrected, and a high-resolution image is obtained by processing the restored data with the conventional imaging method [23] and autofocus [24]. The effectiveness and the practicability of the proposed method are demonstrated by the measured data.

The organization of this paper is as follows: Section II analyzes the data recovery method based on CS. In Section III, the autofocus method of sub-aperture is introduced. In Section IV, the process of restoring the phase error data using CS is researched. Section V presents the signal processing flow of the algorithm. In Section VI, processing of the measured data validates the effectiveness of the proposed method. Finally, we make some conclusions in Section VII.

II. THE DATA RECOVERY METHOD BASED ON CS

A. ZERO PADDING AND MOTION COMPENSATION

For the missing data of strip-map SAR, we first fill the missing data by zero padding prior to the following processing.

For the moving platform, there often exists motion error, which causes serious degradations in the final images [25], so the trajectory deviations must be compensated before imaging. The phase error due to the trajectory deviations in x and y directions can be written as [26].

$$\phi(t,\theta) = \frac{4\pi}{\lambda}\left(-\Delta x(t)\sin(\theta) + \Delta y(t)\cos(\theta)\right) \quad (1)$$

In (1), $\Delta x(t)$ and $\Delta y(t)$ are the trajectory deviations in x and y directions respectively, and θ represents the incidence angle, which is written as shown in (2)

$$\theta_k = \cos^{-1}\left(\frac{H}{R_0 + k\cdot\Delta R}\right) \quad (2)$$

where H represents the height of the plane above the topography, R_0 is the range to the reference point, and ΔR is the range bin size.

B. SUB-APERTURE SEGMENTATION

The pulse number of strip-map data is far beyond the data recovery capacity of CS and the computational complexity is far beyond current hardware computational ability, so it is the next step to divide the strip-map data into several non-overlapping sub-apertures which are processed by algorithms of the spotlight mode. According to the data characteristics of the strip-map and the spotlight [27], the sub-aperture data segmentation scheme is shown in Fig. 1.

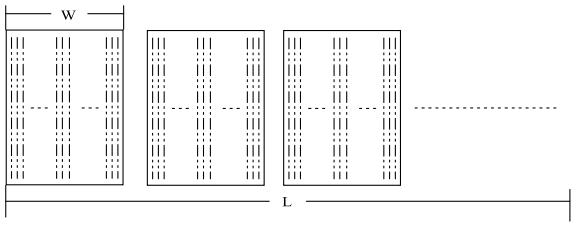

FIGURE 1. The sub-aperture segmentation of the original data.

where L is the pulse number of the whole aperture, the number of sub-apertures is $J = L/W$, W is the pulse number of the sub-aperture, which range is normally as

$$(PRF)^2 \Big/ (2\cdot K_a) \le W \le (PRF)^2 \Big/ K_a \quad (3)$$

In (3), PRF is the pulse repetition frequency, and K_a is the azimuth chirp rate.

In the following section, in order to demonstrate the advantage for the division of the aperture, the computational complexity after sub-aperture segmentation and original data is compared.

Suppose that S is an arbitrary k-sparse signal in C^N and the sparse measurement vector has M samples. The complexity of OMP (the reconstruction algorithm in this paper) is around O (kMN) [13].

Assume that the azimuth pulse number of the sub-aperture is N, the available pulse number is M(M<N), and the sub-aperture is a k-sparse signal, so the original data has JN components, the available pulse number is JM and the original

aperture is a Jk-sparse signal. The total cost of sub-aperture segmentation is $O(JkMN)$ and that of the original aperture is $O\left(J^3kMN\right)$.

C. SUB-APERTURE PREPROCESSING

For each sub-aperture, we can not directly restore the missing data using CS, where preprocessing is needed. For each sub-aperture, we perform reconstruction in the image domain. The processing is as follows.

The radar transmits a Linear Frequency Modulated (LFM) signal with chirp rate k, the 2-D echo signal reflected from the targets is

$$\boldsymbol{S}(t,\tau)=\sigma\cdot rect(\frac{t}{T_a})rect(\frac{\tau-2R_a/c}{T_r}) \cdot \exp\left(j\pi k\left(\tau-2R_a/c\right)^2\right)\cdot\exp\left(-j\frac{4\pi f_c}{c}R_a\right) \quad (4)$$

where $rect(\cdot)$ represents the time window, which is a rectangular function, t is the slow (azimuth) time, T_a is the azimuth aperture time of sub-aperture, τ is the fast (range) time, c is the light velocity, T_r is pulse duration, f_c is carrier frequency, R_a is the distance from the target to the antenna phase center, and σ is the target reflection coefficient.

Performing range Fourier transform, matching filter and motion compensating on Eq. (4), we can obtain [27], [28]

$$\boldsymbol{S}(t,f_\tau)=rect(\frac{t}{T_a})\cdot rect(\frac{f_\tau}{B})\cdot\sigma \cdot\exp\left(-j\frac{4\pi\left(f_c+f_\tau\right)}{c}\left(R_a-R_0\right)\right) \quad (5)$$

where R_0 is the distance between the antenna phase center and the sub-aperture imaging center, and $B=KT_r$ is the bandwidth of the transmitted signal.

Performing range inverse Fourier transform on Eq. (5), we can obtain

$$\boldsymbol{S}(t,f_\tau)=\sigma\cdot B\cdot rect(\frac{t}{T_a}) \cdot Sinc\left\{B\left[\tau-\frac{2}{c}\left(R_a(t)-R_0\right)\right]\right\} \cdot\exp\left(-j\frac{4\pi f_c}{c}\left(R_a(t)-R_0\right)\right) \quad (6)$$

After range compression, we can reconstruct the image in azimuth based on CS.

D. SUB-APERTURE RECONSTRUCTION BASED ON CS

If the radar echo reflection intensities of some patches are much stronger than other patches in the imaging area, or the targets occupy a tiny fraction of the whole imaging area, we assume that the scene is sparse [17], [29].

Because we perform imaging in the azimuth frequency domain, which meets the sparse requirement, this paper utilizes the Fourier Basis as the Base Matrix.

Assume that the azimuth pulse number of the sub-aperture is N and the available pulse number is M ($M<N$), the missing pulse number is $N-M$. Firstly, we establish the azimuth basis matrix $\boldsymbol{\varphi}=\{\varphi_0,\varphi_1,\ldots,\varphi_{N-1}\}_{N\times N}$:

$$\varphi_n=\exp(-j2\pi\cdot(n\cdot\Delta f_a-\frac{PRF}{2})\cdot n'\cdot\Delta t_a) \quad (0\le n'\le N-1) \quad (7)$$

where φ_n is the column vector, $\Delta f_a=\frac{PRF}{N}$ is the azimuth frequency interval, and $\Delta t_a=\frac{1}{PRF}$ is the pulse repetition interval.

The $M\times N$ azimuth measurement matrix $\boldsymbol{A}$ is made up of M lines from a $N\times N$ unit matrix. The location of the M lines corresponds to the location of the available echo pulse. The azimuth measurement vector of each range is expressed as:

$$S_a=\boldsymbol{A}\varphi\theta_a \quad (8)$$

In (8), θ_a is the azimuth sparse vector, namely the image reconstructed in azimuth frequency domain for each range unit. CS reconstruction can replace the Fourier transform of Eq. (6).

Carrying out the reconstruction processing of each range unit with the OMP algorithm iteratively, we get the reconstructed image of each sub-aperture.

After performing azimuth inverse Fourier transform on the reconstructed image, the range compressed data is obtained. So far, the missing pulse data has been restored and the azimuth data has been restored completely. Then range Fourier transform is performed on the range compressed data, and multiply the data with the following formula (9). We can obtain the complete data of each sub-aperture after performing range inverse Fourier transform.

$$\boldsymbol{S}_{ref}(t,f_\tau)=\exp(-j\pi\frac{f_\tau^2}{k})\cdot\exp\left(-j\frac{4\pi\left(f_c+f_\tau\right)}{c}R_0\right) \quad (9)$$

E. SUB-APERTURE RECOMBINING

Because there is no overlap between the sub-apertures, the integrated strip-map data can be directly obtained by recombining all sub-apertures in sequential order.

III. SUB-APERTURE AUTOFOCUS

There often exist phase error, which leads to defocus in azimuth, and fail to satisfy the sparse requirement of CS theory. Even if the scene is sparse, it is impossible to reconstruct the image. Therefore before reconstructing the sub-aperture image based on CS, we should perform autofocus on each sub-aperture data.

Because the missing data is sparse in azimuth, if we transform the missing data into frequency domain by setting the damaged or missing data to zero, the obtained images are greatly defocused. The performance of PGA [30] and ROPE [31] algorithms will not be ideal. The EMMLE algorithm [32] can get better focusing performance without a window, but it is a computational expensive task and also limits the engineering application. This paper selects the PAST algorithm [33] to estimate the phase error of the sub-aperture, which avoids the procedures of covariance matrix estimation and eigenvector decomposition of the EMMLE algorithm.

Literature [33] introduces the PAST algorithm of full data in details. For the missing data, we need to do some improvement on PAST algorithm, the processing is as follows.

Step 1: Remove the data of zero padding position and calculate the corresponding eigenvector of the largest eigenvalue by the PAST algorithm.

Step 2: Extract the phase part (phase error) of the eigenvector according to formula (10).

$$Error_{phase} = \frac{Vector_{Max}}{|Vector_{Max}|} \tag{10}$$

where $Error_{phase}$ is the phase error, $Vector_{Max}$ presents the corresponding eigenvector of the largest eigenvalue.

Step 3: Compensate the phase error of the missing data according to formula (11).

$$Data_{after} = Data_{before} \cdot conj(Error_{phase}) \tag{11}$$

In (11), $Data_{before}$ and $Data_{after}$ are the sub-aperture data before and after autofocus, and $conj(\cdot)$ represents taking the conjugate of the content in bracket.

Step 4: Get an initial image by inserting zeroes and performing Fourier transform for the azimuth missing data. Perform inverse Fourier transform after moving the strongest scattering point to the Doppler zero point for each range gate.

Step 5: Transform the image back into the data domain, and remove the data of zero padding position.

Step 6: Extract the corresponding eigenvector of the largest eigenvalue by the PAST algorithm and extract the phase part of the eigenvector and compensate the phase error of the missing data.

Step 7: Repeat the third to the sixth step, until it meets the end condition of the iteration.

After performing the above steps, the phase error is compensated. The accuracy of reconstructed image based on CS is guaranteed.

IV. PHASE ERROR SIGNAL RECOVERY

When the sub-aperture is autofocused, there is unknown linear phase [24]. It will cause ghost images for the strip-map data to recombine directly the recovered sub-aperture data after autofocus. Therefore before combining the sub-aperture data, it is necessary to recover the phase error signal compensated by autofocus, in order to ensure the accuracy and integrity.

The phase error signal of the original missing data is non-continuous, as shown in Fig. 2.

From Fig. 2, the phase error is non-continuous because of the non-continuous for the missing pulse position in raw data.

We have recovered the missing data entirely by CS, so the non-continuous phase error signal can not be used to compensate the continuous data. This paper proposes a method which recovers the phase error signal by CS to turn non-continuous phase error signal into continuous signal. The process is as follows.

First, we perform Fourier transform on the same range gate signals before and after PAST autofocus for each

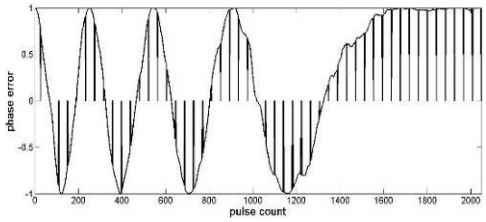

FIGURE 2. The phase error signal of the missing data.

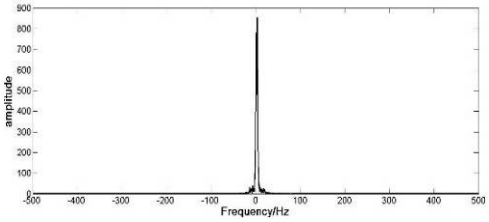

FIGURE 3. The frequency domain signal of the phase error.

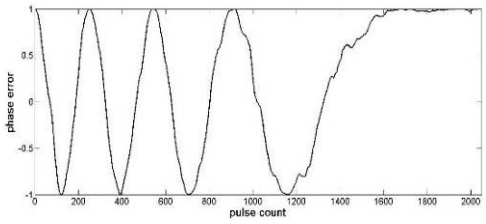

FIGURE 4. The CS recovery phase error signal.

sub-aperture, then conjugate multiplication will be applied to the signal. The phase error signal of missing data will be obtained. It is shown in (12)

$$\Theta = \text{fft}(S_1) \cdot \text{conj}(\text{fft}(S_2)) \tag{12}$$

where S_1 and S_2 are the corresponding signals before and after autofocus of the same range gate respectively, $\text{fft}(\cdot)$ represents performing Fourier transform on the content in bracket.

Θ still is a sparse signal in frequency domain, as shown in Fig. 3.

The phase error signal is reconstructed sparsely in the frequency domain with the basis matrix $\boldsymbol{\varphi}$ and the measurement matrix $\boldsymbol{A}$ introduced in section II.D.

$$\Theta = \boldsymbol{A}\boldsymbol{\varphi}\phi \tag{13}$$

where, ϕ is the frequency domain sparse vector of Θ. After sparsely reconstructing with the OMP algorithm, we perform inverse Fourier transform for ϕ. The complete phase error signal can be obtained, as shown in Fig. 4.

To compare the Fig. 2 and 4, we find that the phase error signal is changed from non-continuous to continuous after CS recovery.

V. ALGORITHM FLOW

The algorithm flow of the high-resolution imaging method presented in this paper is shown in Fig. 5.

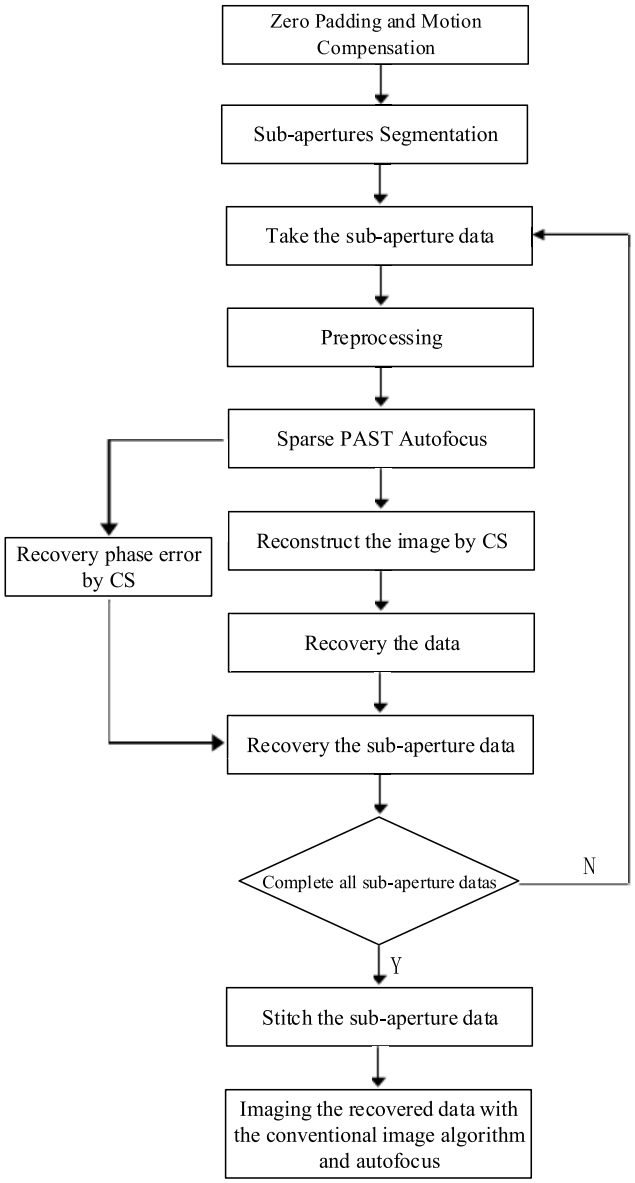

FIGURE 5. Algorithm processing flowchart.

VI. THE MEASURED DATA PROCESSING RESULTS AND ANALYSIS

The paper firstly takes the measured data of a certain type of helicopter airborne SAR as an example in order to analyze the imaging results of the proposed algorithm. The major radar parameters are as follows: radar carrier frequency $f_c = 10GHz$, signal band width $B = 1GHz$, range sampling rate $f_s = 1.2GHz$, pulse width $\tau = 15\mu s$, and pulse repetition frequency $PRF = 2000Hz$. The pulse number of the entire aperture is 16,384, and the pulse number of the sub-aperture is 2048. As this type of helicopter radar is located at the top of the helicopter rotor, it is subject to rotor blocking effect, and the received echoes are disturbed, which results in missing echo data.

The original missing radar echo data of the helicopter SAR is shown in Fig. 6.

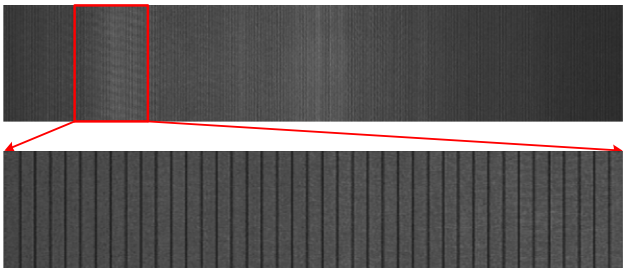

FIGURE 6. Original missing echo data.

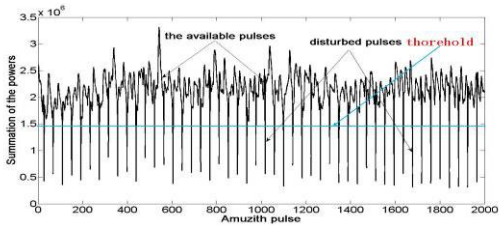

FIGURE 7. Power summations of each pulse.

FIGURE 8. Sub-aperture image reconstructed using CS.

In Fig. 6, there are dark stripes. In order to demonstrate the dark stripes of the interfered data distinctly, the zoomed in original data of the above marked areas is shown. It is found from Fig. 6 that the power of the interfered data is lower than that of the undisturbed data. The dark stripes in the strips are the interfered pulses. The power summations of each pulse are shown in Fig. 7.

It can be seen from Fig. 7 that the disturbed pulse power is significantly weaker than the available pulse. The positions of the disturbed pulses can be distinguished according to the difference of the power, which is below the threshold. The threshold is defined as

$$Thre = \frac{Power_{Max} + Power_{Min}}{2} \tag{14}$$

In (14), $Thre$ presents the value of the threshold, $Power_{Max}$ is the max value of the power summations, $Power_{Min}$ is the min value.

The sub-aperture image reconstructed using CS from Fig. 6 is shown in Fig. 8.

The sub-aperture data recovered using CS is shown in Fig. 9.

It can be seen from Fig. 9 that there is no damaged pulse data in the sub-aperture data, and all the data are recovered. The strip-map data can be obtained by recombining the sub-aperture data, which is shown in Fig.10.

It can be seen through the comparison of Figs. 10 and 6 that the original missing data has been fully recovered.

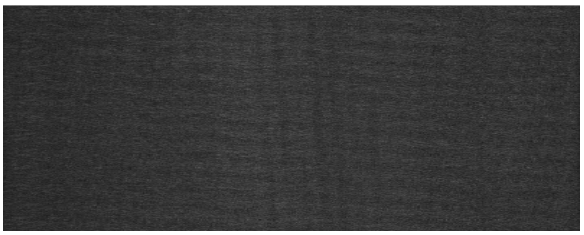

FIGURE 9. Recovered sub-aperture data using CS.

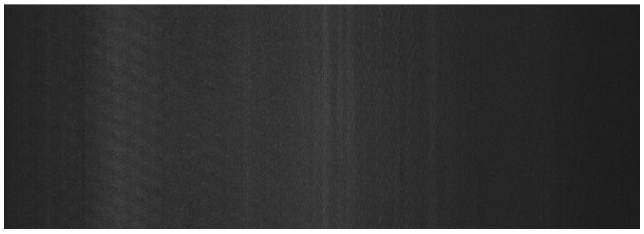

FIGURE 10. Recovered full aperture data.

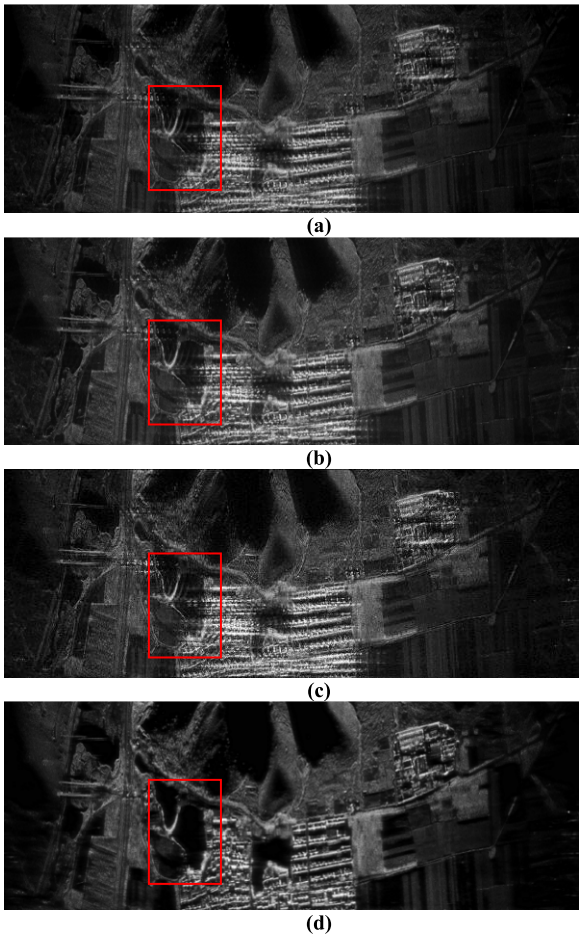

FIGURE 11. Imaging results of the strip-map data: (a) Image of the original missing data, (b) Image of the interpolation recovered data, (c) Image of GAPES recovered data and (d) Image of the proposed method in this paper.

The imaging results of the original missing data, interpolation recovery data, GAPES recovered data and the proposed method are shown in Fig.11.

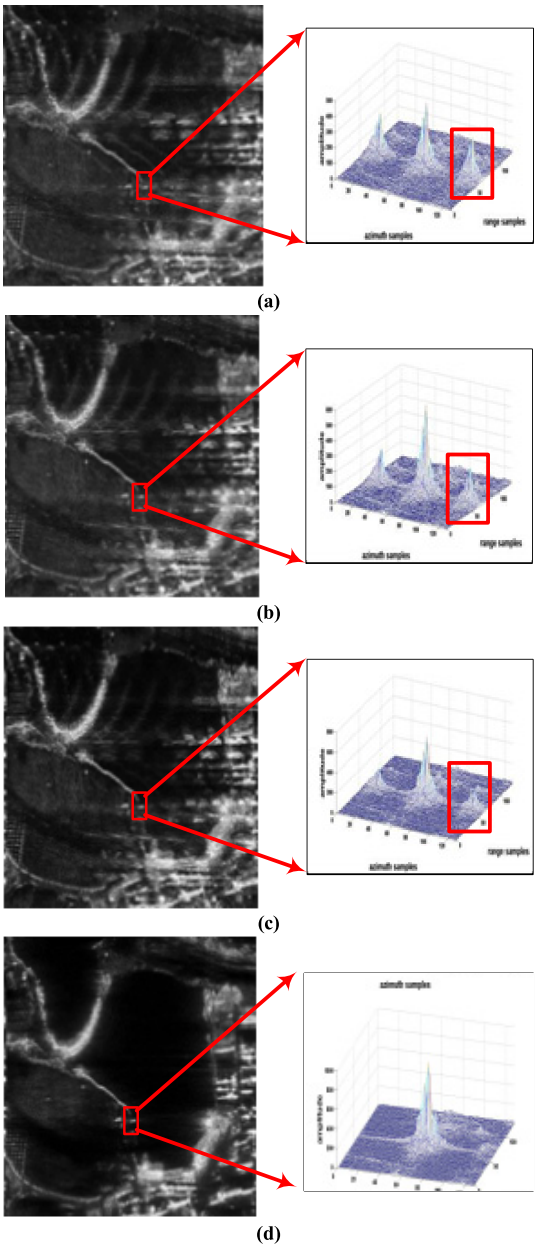

FIGURE 12. The zoomed in images of the marked areas: (a) Image of the original missing data, (b) Image of the interpolation recovered data,(c) Image of GAPES recovered data and (d) Image of the proposed method in this paper.

Fig. 11 (a) shows the image of the original missing data. Fig. 11 (b) shows the image of the interpolation recovery data with Sinc interpolation. Fig. 11 (c) shows the image of the GAPES recovery data using the 100 pulses in the neighborhood of the missing data. Fig. 11 (d) shows the image of the missing pulse data recovered with the proposed method. In the following section, through the zoomed in images of the above marked areas, comparison is made among these methods.

By comparing the four images in Figs. 11 and 12, it can be seen that, due to the loss of the pulse data, the image quality of the original data degrades significantly. The ghost images are

TABLE 1. Image entropy value.

IMAGE	Entropy value
Original missing data imaging result	16.0269
Imaging result of the interpolation-recovered data	15.9959
Imaging result of the GAPES-recovered data	15.8861
Imaging result of the method proposed in this paper	13.2792

very apparent. Although the interpolation method somewhat improves the result, the obtained image is smeared with the ghost images. Due to the fact that the GAPES recovery method adopts the 100 pulses in the neighborhood of the missing data to recover the missing data, its computational quantity is acceptable. However, the spectral width of the 100 pulses is far narrower than that of the entire aperture, the GAPES recovered data does not include all of the spectral information of the missing data. Although the imaging quality is improved, the ghost images are still present. The proposed method overcomes the ghost images of the original the missing data, improves the image quality, and achieves a high-resolution image with excellent focusing.

In the following section, in order to show the performance of the proposed algorithm, the image quality is quantitatively evaluated by the image entropy values.

The entropy of the 2-D SAR image is defined as follows:

$$E(P) = -\sum_{i=0}^{Na-1}\sum_{j=0}^{Nr-1} P(i,j)\cdot \ln(P(i,j)) \tag{15}$$

where Na is the azimuth number of the image, Nr is the range number of the image, and $P(i,j)$ is the scattering intensity density of the image, which is defined as:

$$P(i,j) = \frac{|S(i,j)|^2}{Q(S)} \tag{16}$$

where $Q(S)$ is the total energy of the image, which is defined as

$$Q(S) = \sum_{i=0}^{Na-1}\sum_{j=0}^{Nr-1} |S(i,j)|^2 \tag{17}$$

where $S(i,j)$ is the reflection intensity of each point in the image.

Regarding the imaging result of the same data, the clearer the image is, the smaller the corresponding entropy value is, and the more blurred the image is, the greater the entropy value is. The entropy values of the four whole images in Fig.11 are shown in Table 1.

To compare of the entropy values of the four images, we can find that the entropy value of the SAR image obtained by the proposed algorithm is significantly smaller than those of the other three images, thus it is proved that the proposed algorithm greatly enhances the imaging quality of the strip-map missing data.

TABLE 2. The contrast of the four images.

Image	The image contrast
Original missing data imaging result	48.556838
Imaging result of the interpolation-recovered data	68.998357
Imaging result of the GAPES-recovered data	74.104182
Imaging result of the method proposed in this paper	102.24616

For further quantifying the comparison results, another evaluation indicator is applied i.e., the contrast of image.

The contrast of the 2-D SAR image is defined as follows:

$$Q(S) = \sum_{i=0}^{Na-1}\sum_{j=0}^{Nr-1} |\delta(i,j)|^2 p_\delta(i,j) \tag{18}$$

where

$$\delta(i,j) = ||S(i,j)| - |S_r(i,j)|| \tag{19}$$

where $S(i,j)$ and $S_r(i,j)$ is the reflection intensity of each point and the four points around it, $p_\delta(i,j)$ is the distribution probability which gray difference between adjacent pixels is $\delta(i,j)$.

The contrasts of the four whole images in Fig.11 are shown in Table 2.

From the table 2, the excellent performance of the proposed method is further demonstrated.

In order to further validate our method, we provided the performance of another group measured data with stronger targets.

The major parameters of the radar are as follows: radar carrier frequency $f_c = 10GHz$, signal band width $B = 300MHz$, range sampling rate $f_s = 400MHz$, pulse width $\tau = 7.5\mu s$, and pulse repetition frequency $PRF = 500Hz$. The pulse number of the entire aperture is 8192, and the pulse number of sub-aperture is 1024.

The imaging results of the four methods are shown in Fig. 13.

The entropy values of the four whole images in Fig. 13 are shown in Table 3.

The contrasts of the four whole images in Fig. 13 are shown in Table 4.

The results of Fig. 13, Table 3 and Table 4 demonstrate the excellent performance of the proposed method against other three methods with stronger targets. Fig. 13 shows that the proposed method has better image quality compared with the other three methods.

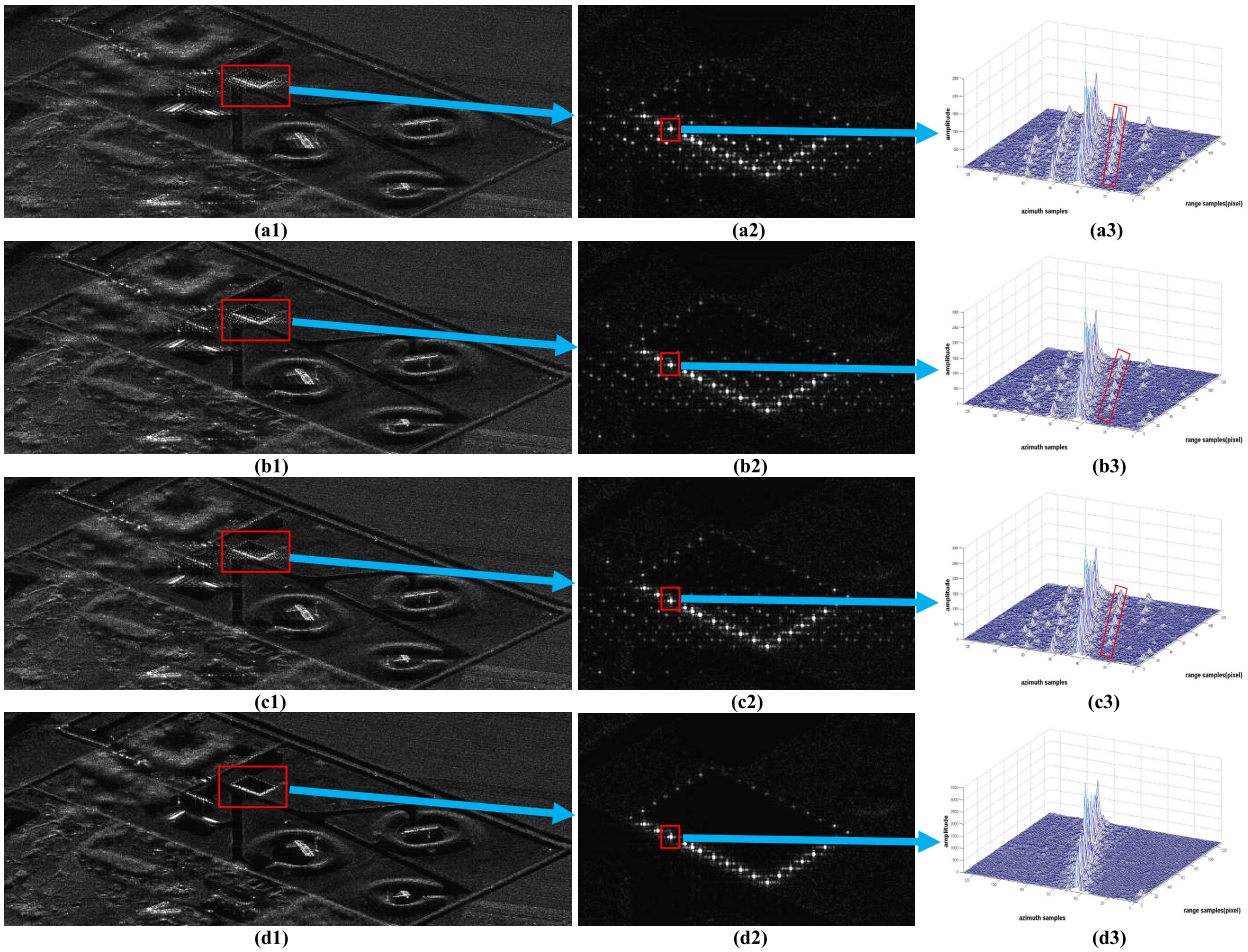

FIGURE 13. Imaging results of the strip-map data: (a1) Image of the original missing data, (a2)The zoomed in images of the marked areas, (a3)The 3-D amplitude maps of the marked areas, (b1) Image of the interpolation recovered data, (b2)The zoomed in images of the marked areas, (b3)The 3-D amplitude maps of the marked areas, (c1) Image of GAPES recovered data, (c2)The zoomed in images of the marked areas, (c3)The 3-D amplitude maps of the marked areas, (d1) Image of the method proposed in this paper, (d2)The zoomed in images of the marked areas, (d3)The 3-D amplitude maps of the marked areas.

TABLE 3. Image entropy value.

IMAGE	Entropy value
Original missing data imaging result	14.161698
Imaging result of the interpolation-recovered data	14.098161
Imaging result of the GAPES-recovered data	14.074674
Imaging result of the method proposed in this paper	13.865479

TABLE 4. The contrasts of the four images.

Image	The image contrast
Original missing data imaging result	1200.4401
Imaging result of the interpolation-recovered data	1358.2924
Imaging result of the GAPES-recovered data	1397.7981
Imaging result of the method proposed in this paper	1613.3577

VII. CONCLUSION

This paper proposes a high-resolution imaging method for strip-map SAR with missing data based on compressed sensing. First, the strip-map missing data is divided into several sub-apertures in order to reduce the data amount and the computational complexity, then the intact sub-aperture data is recovered with CS. The full strip-map data are obtained by combining the sub-aperture data. Through the sparse PAST algorithm, autofocus is performed on each sub-aperture, thus ensuring the sparse requirement of the reconstructed image. The missing phase error signal is recovered using CS, in order to ensure the correctness of the sub-apertures combining. The results of the measured data indicate that the method detailed in this paper ensures the correctness of the data recovery and resolves the ghost images for strip-map SAR with missing data. The entropy value and the contrast of the image from the

proposed method are markedly better than those of the other three imaging results, which proves that the proposed method enhances the imaging quality of the strip-map missing data, and also proves that the proposed method is feasible and effective.

REFERENCES

[1] E. G. Larsson, G. Liu, P. Stoica, and J. Li, "High-resolution SAR imaging with angular diversity," *IEEE Trans. Aerosp. Electron. Syst.*, vol. 37, no. 4, pp. 1359–1372, Oct. 2001.
[2] G. O. Glentis, K. Zhao, A. Jakobsson, and J. Li, "Non-parametric high-resolution SAR imaging," *IEEE Trans. Signal Process.*, vol. 61, no. 7, pp. 1614–1624, Apr. 2013.
[3] X. Du, C. Duan, and W. Hu, "Sparse representation based autofocusing technique for ISAR images," *IEEE Trans. Geosci. Remote Sens.*, vol. 51, no. 3, pp. 1826–1835, Mar. 2013.
[4] X. Bai, F. Zhou, Z. Bao, and M. Xing, "High-resolution radar imaging of air targets from sparse azimuth data," *IEEE Trans. Aerosp. Electron. Syst.*, vol. 48, no. 2, pp. 1643–1655, Apr. 2012.
[5] A. V. Oppenheim, *Signal and System*, 2nd ed. Beijing, China: Publishing House of Elecronincs Industry, 2010.
[6] I. J. Gupta, "High-resolution radar imaging using 2-D linear prediction," *IEEE Trans. Antennas Propag.*, vol. 42, no. 1, pp. 31–37, Jan. 1994.
[7] I. J. Gupta, M. J. Beals, and A. Moghaddar, "Data extrapolation for high resolution radar imaging," *IEEE Trans. Antennas Propag.*, vol. 42, no. 11, pp. 1540–1545 Nov. 1994.
[8] I. Erer, "A new data extrapolation algorithm for high resolution ISAR imaging," *AEU-Int. J. Electron. Commun.*, vol. 60, no. 4, pp. 316–319, 2006.
[9] P. Stoica, E. G. Larsson, and J. Li, "Adaptive filter-bank approach to restoration and spectral analysis of gapped data," *Astronommical J.*, vol. 120, pp. 2163–2173, Oct. 2000.
[10] E. G. Larsson, P. Stoica, and J. Li, "Amplitude spectrum estimation for two-dimensional gapped data," *IEEE Trans. Signal Process.*, vol. 50, no. 6, pp. 1343–1354, Jun. 2002.
[11] P. Stoica, J. Li, and J. Ling, "Missing data revovery via a nonparametric iterative adaptive approach," *IEEE Signal Process. Lett.*, vol. 16, no. 4, pp. 241–244, Apr. 2009.
[12] R. G. Baraniuk, "Compressive sensing," *IEEE Signal Process. Mag.*, vol. 24, no. 4, pp. 118–124, Jul. 2007.
[13] J. A. Tropp and A. C. Gilbert, "Signal recovery from random measurements via orthogonal matching pursuit," *IEEE Trans. Inf. Theory*, vol. 53, no. 12, pp. 4655–4666, Dec. 2007.
[14] J. Fang, Z. Xu, B. Zhang, W. Hong, and Y. Wu, "Fast compressed sensing SAR imaging based on approximated observation," *IEEE J. Sel. Topics Appl. Earth Observ. Remote Sens.*, vol. 7, no. 1, pp. 352–363, Jan. 2014.
[15] J. Yang, J. Thompson, X. Huang, T. Jin, and Z. Zhou, "Random-frequency SAR imaging based on compressed sensing," *IEEE Trans. Geosci. Remote Sens.*, vol. 51, no. 2, pp. 983–994, Feb. 2013.
[16] J. Yang, X. Huang, T. Jin, J. Thompson, and Z. Zhou, "Synthetic aperture radar imaging using stepped frequency waveform," *IEEE Trans. Geosci. Remote Sens.*, vol. 50, no. 5, pp. 2026–2036, May 2012.
[17] L. C. Potter, E. Ertin, J. T. Parker, and M. Cetin, "Sparsity and compressed sensing in radar imaging," *Proc. IEEE*, vol. 98, no. 6, pp. 1006–1020, Jun. 2010.
[18] M. T. Alonso, P. Lopez-Dekker, and J. J. Mallorqui, "A novel strategy for radar imaging based on compressive sensing," *IEEE Trans. Geosci. Remote Sens.*, vol. 48, no. 12, pp. 4285–4295, Dec. 2010.
[19] V. M. Patel, G. R. Easley, D. M. Healy, Jr., and R. Chellappa, "Compressed synthetic aperture radar," *IEEE J. Sel. Topics Signal Process.*, vol. 4, no. 2, pp. 244–254, Apr. 2010.
[20] J. Yang, T. Jin, and X. Huang, "Compressed sensing radar imaging with magnitude sparse representation," *IEEE Access*, vol. 5, pp. 29722–29733, 2019.
[21] J. Yang, J. Thompson, X. Huang, T. Jin, and Z. Zhou, "Segmented reconstruction for compressed sensing SAR imaging," *IEEE Trans. Geosci. Remote Sens.*, vol. 51, no. 7, pp. 4214–4225, Jul. 2013.
[22] W. W. Wang *et al.*, "An imaging method based on compressed sensing for sparse aperture of SAR," *Acta Electron. Sinica*, vol. 40, no. 12, pp. 2487–2494, Dec. 2012.
[23] I. G. Cumming and F. H. Wong, *Digital Processing of Synthetic Aperture Radar Data: Algorithms and Implementation*. Beijing, China: Publishing House of Electronics Industry, 2012.
[24] R. Jiang, D. Y. Zhu, and Z. D. Zhu, "A novel approach to strip-map SAR autofucos," *Acta Aeronautica Astronautica Sinica*, vol. 31, no. 12, pp. 2385–2392, Dec. 2012.
[25] W. Pu, Y. Huang, H. Yang, J. Yang, and J. Wu, "Fast compressive sensing-based SAR imaging integrated with motion compensation," *IEEE Access*, vol. 5, pp. 53284–53295, 2019.
[26] D. G. Thompson, J. S. Bates, and D. V. Arnold, "Extending the phase gradient autofocus algorithm for low-altitude stripmap mode SAR," in *Proc. Hamburg IEEE Int. Geosci. Remote Sens. Symp. (IGARSS)*, Apr. 1999, pp. 564–566.
[27] W. G. Carrara, R. E. Goodman, and R. M. Majewski, *Spotlight Synthetic Aperture Radar: Signal Processing Algorithms*. Boston, MA, USA: Artech House, 1995.
[28] D. A. Ausherman, A. Kozma, H. M. Jones, E. C. Poggio, and J. L. Walker, "Developments in radar imaging," *IEEE Trans. Aerosp. Electron. Syst.*, vol. AES-20, no. 4, pp. 363–400, Jul. 1984.
[29] R. Baraniuk and P. Steeghs, "Compressive radar imaging," in *Proc. IEEE Radar Conf.*, Apr. 2007, vol. 17, no. 20, pp. 128–133.
[30] D. E. Wahl, F. H. Eichel, D. C. Ghiglia, and C. V. Jakowatz, "Phase gradient autofocus—A robust tool for high resolution SAR phase correction," *IEEE Trans. Aerosp. Electron. Syst.*, vol. 30, no. 3, pp. 827–835, Jul. 1994.
[31] C. A. Snarski, "Rank one phase error estimation for range-Doppler imaging," *IEEE Trans. Aerosp. Electron. Syst.*, vol. 32, no. 2, pp. 676–688, Apr. 1996.
[32] X. Yu and D. Y. Zhu, "A motion compensation algorithm for 2-dimensional compressed ISAR imaging," *Acta Electron. Sinica*, vol. 40, no. 9, pp. 1783–1789, Sep. 2012.
[33] R. Jiang, D. Y. Zhu, M. W. Shen, and Z. D. Zhu, "An autofocus algorithm for spotlight SAR imagery using the projection approximation subspace tracking approach," *Acta Electron. Sinica*, vol. 40, no. 6, pp. 1251–1256, Jun. 2012.

HUAJUN DUAN was born in Shandong, China, in 1976. He received the B.S degree in communication engineering, in 2001. He is currently pursuing the Ph.D. degree with NUAA.

His research interests include radar sparse imaging and radar imaging algorithms.

DAIYIN ZHU was born in Wuxi, China, in 1974. He received the B.S. degree in electronic engineering from Southeast University, Nanjing, China, in 1996, and the M.S. and Ph.D. degrees in electronics from the Nanjing University of Aeronautics and Astronautics (NUAA), Nanjing, in 1998 and 2002, respectively.

From 1998 to 1999, he was a Guest Scientist with the Institute of Radio Frequency Technology, German Aerospace Center, Oberphaffenhofen, where he worked in the field of SAR interferometry. In 1998, he joined the Department of Electronic Engineering, NUAA, where he is currently a Professor. He has developed algorithms for several operational airborne SAR systems. His current research interests include radar imaging algorithms, SAR/ISAR autofocus techniques, SAR ground moving target indication (SAR/GMTI), and SAR interferometry.

TIANSHUN XIANG was born in Shannxi, China, in 1990. He received the B.S degree in communication engineering from Anhui University, Hefei, China, in 2012. He is currently pursuing the Ph.D. degree with NUAA. His research interests include radar imaging algorithms and motion compensation algorithms.